TWO NEW BOUNDARY CONDITIONS FOR USE WITH THE MAXIMUM ENTROPY CLOSURE AND AN APPROXIMATE RIEMANN SOLVER

Thomas A. Brunner and James P. Holloway
University of Michigan
2355 Bonisteel Boulevard
Ann Arbor, Michigan 48109-2014
tbrunner@umich.edu; hagar@umich.edu

ABSTRACT

The maximum entropy closure for the two-moment approximation of the neutron transport equation is presented. We use a robust Roe-type Riemann solver to solve the resulting moment equations. We have developed three boundary conditions to use with this method. The ghost cell method effectively implements the Mark boundary condition by placing phantom cells just outside the physical system. This method is extremely simple to implement and gives reasonable results. The boundary Eddington factor method implements the Marshak boundary condition. While it yields good results at boundaries with incoming neutrons, it does not do so well at vacuum boundaries. The partial numerical flux method is an extension of the Marshak boundary condition, allowing us to specify extra angular information about the incoming neutron distribution. The neutron flux calculated with this method are the generally the best out of the three boundary conditions presented here.

1 INTRODUCTION

Approximations to neutral particle transport are often based on only the first two moments of the angular flux ψ, namely the scalar flux ϕ and the net current J. These moments satisfy the equation

$$\frac{\partial}{\partial t}\begin{bmatrix}\phi\\ J\end{bmatrix}+\frac{\partial}{\partial x}\begin{bmatrix}J\\ \chi\phi\end{bmatrix}=-\begin{bmatrix}\Sigma_a\phi\\ \Sigma_t J\end{bmatrix}+\begin{bmatrix}S_0\\ S_1\end{bmatrix}, \tag{1}$$

where χ is the normalized second moment, or Eddington factor,

$$\chi=\frac{1}{\phi}\int_{-1}^{1}\mu^2\psi(\mu)d\mu\,. \tag{2}$$

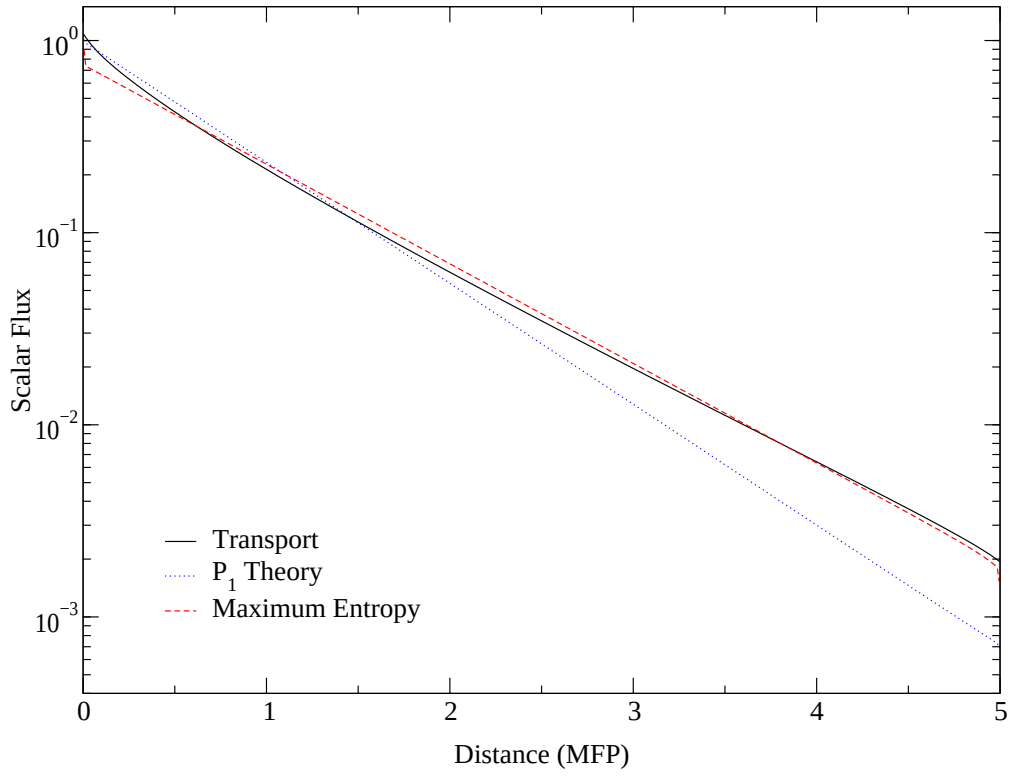

Figure 1: Scalar flux in a semi-infinite slab calculated using the maximum entropy closure, P_1 theory, and a transport solution. Isotropic incoming source at $x = 0$, vacuum boundary at $x = 5$ mean free paths. The scattering ratio is $c = 0.3$.

In previous summaries,[1,2] we described numerical methods for working with a non-linear closure first proposed by Minerbo[3] for photon transport; in one dimension this closure is

$$\psi(x,\mu) = \phi(x)\frac{b(x)}{2\sinh b(x)}\, e^{b(x)\mu}, \tag{3}$$

where b is related to ϕ and J by

$$\frac{J}{\phi} = \frac{\cosh b}{\sinh b} - \frac{1}{b}\,. \tag{4}$$

Figure 1 shows that the maximum entropy closure agrees well with a transport calculation where P_1 does not.

Riemann solvers[4–6] are a class of conservative finite volume methods wherein the net flow, $\mathbf{F} = [J, \chi\phi]^T$, of particles and momentum across the cell interfaces is computed by solving an idealized conservation law exactly near each interface. This flow $\mathbf{F}$ is called the flux in the Riemann solver community; we will call it the numerical flux in order to distinguish it from the standard nuclear engineering flux ϕ. In previous calculations[1,2] we implemented only vacuum boundary conditions, and did so by filling flanking ghost cells with nothing. Two new boundary conditions are presented here; all three provide a way to drive the problem with a incoming boundary flux.

1.1 DERIVATION OF THE MAXIMUM ENTROPY CLOSURE

In a two moment approximation, we use only the first two angular moments to describe the angular flux. Here we would like to derive the most likely form of ψ which is consistent with these two moments.

1.1.1 Entropy

The distribution which maximizes entropy would be this most likely distribution. We will define entropy, H, as

$$H(\psi) = \int_{4\pi} \psi \ln \psi \, d\mathbf{\Omega} \tag{5}$$

without the conventional minus sign since it will make no difference in determining extreme points. To maximize the entropy with the given values of the first two moments we introduce Lagrange multipliers and define the constrained entropy, $\tilde{H}$,

$$\tilde{H}(\psi) = \int_{4\pi} \psi \ln \psi \, d\mathbf{\Omega} \, + C_1 \left[\int_{4\pi} \psi \, d\mathbf{\Omega} \, - \phi \right] + \mathbf{C}_2 \cdot \left[\int_{4\pi} \psi \mathbf{\Omega} \, d\mathbf{\Omega} \, - \mathbf{J} \right] \tag{6}$$

where C_1 and $\mathbf{C}_2$ are Lagrange multipliers. We now must find the ψ which gives us an extreme point of $\tilde{H}$. Write ψ as

$$\psi = \psi_0 + \delta\psi \, , \tag{7}$$

where ψ_0 is the distribution which has the extreme entropy and $\delta\psi$ is a small arbitrary variation to it. We can now expand $\tilde{H}(\psi)$ about ψ_0,

$$\tilde{H}(\psi_0 + \delta\psi) = H(\psi_0) + \frac{\partial \tilde{H}}{\partial \psi}(\psi_0)\delta\psi + O\left(|\delta\psi|^2\right) . \tag{8}$$

At the maximum the linear term must be zero.

$$0 = \frac{\partial \tilde{H}}{\partial \psi}(\psi_0)\delta\psi \tag{9}$$

$$= \int_{4\pi} \left(\ln \psi_0 + 1 + C_1 + \mathbf{C}_2 \cdot \mathbf{\Omega} \right) \delta\psi \, d\mathbf{\Omega} \, . \tag{10}$$

We would like this to be true for any $\delta\psi$, which means the rest of the integrand must be zero,

$$0 = \ln \psi_0 + 1 + C_1 + \mathbf{C}_2 \cdot \mathbf{\Omega} \, . \tag{11}$$

Solving for ψ_0 yields

$$\psi_0 = e^{-1-C_1} e^{-\mathbf{C}_2 \cdot \mathbf{\Omega}} \tag{12}$$

$$= a e^{\mathbf{b} \cdot \mathbf{\Omega}} \, , \tag{13}$$

where a and $\mathbf{b}$ are new, more convenient constants.

This form of the angular flux has several nice features. It is always non-negative, which implies the current is flux limited, $|J| < \phi$. It limits to P_1 as $b \to 0$, and as $b \to \infty$, the distribution becomes a beam.

1.1.2 Normalizing the Maximum Entropy Form of the Angular Flux

Now we need to determine what the constants a and $\mathbf{b}$ are in terms of the first two moments of ψ. (The subscript 0 has been dropped.) The constant a can be determined from the zeroth moment of the angular flux.

$$\phi = \int_{4\pi} a e^{\mathbf{b}\cdot\mathbf{\Omega}}\, d\mathbf{\Omega}\,. \tag{14}$$

A useful transformation for many of the integrals is to adjust the pole of $\mathbf{\Omega}$ to be the same as $\mathbf{b}$. In this coordinate system

$$\phi = \int_0^{2\pi}\int_{-1}^{1} a e^{b\mu}\, d\mu\, d\phi \tag{15}$$

$$= 4\pi \frac{a}{b}\sinh b\,, \tag{16}$$

where $b = |\mathbf{b}|$. Solving for a and inserting into Eq. 13 gives us

$$\psi = \phi \frac{b}{4\pi \sinh b} e^{\mathbf{b}\cdot\mathbf{\Omega}}\,. \tag{17}$$

Now we will take the first moment in order to determine $\mathbf{b}$; this gives

$$\mathbf{J} = \phi \frac{b}{4\pi \sinh b}\int_{4\pi} e^{\mathbf{b}\cdot\mathbf{\Omega}}\mathbf{\Omega}\, d\mathbf{\Omega} \tag{18}$$

$$= \phi \frac{\mathbf{b}}{b}\left(\frac{\cosh b}{\sinh b} - \frac{1}{b}\right). \tag{19}$$

While it is impossible to solve for $\mathbf{b}$ analytically, this equation does implicitly define it. Most other important formulas related to this approximation are only functions of the ratio of $\mathbf{J}/\phi$. Rearranging gives us

$$\boldsymbol{\eta} \equiv \frac{\mathbf{J}}{\phi} = \frac{\mathbf{b}}{b}\left(\frac{\cosh b}{\sinh b} - \frac{1}{b}\right). \tag{20}$$

1.1.3 The Second Moment

The first moment equation contains the second moment. The whole point of introducing an approximation is to be able to close the series of moment equations. The second moment in three dimensions (Eq. 2 is 1D) is found by integrating

$$\boldsymbol{\chi} = \frac{1}{\phi}\int_{4\pi} (\mathbf{\Omega}\otimes\mathbf{\Omega})\,\phi \frac{b}{4\pi\sinh b} e^{\mathbf{b}\cdot\mathbf{\Omega}}\, d\mathbf{\Omega}\,. \tag{21}$$

With $\mathbf{\Omega} = \left[\sqrt{1-\mu^2}\cos\phi, \sqrt{1-\mu^2}\sin\phi, \mu\right]^T$, the outer (or Kronecker or tensor) product expands to

$$\mathbf{\Omega}\otimes\mathbf{\Omega} = \begin{bmatrix} (1-\mu^2)\cos^2\phi & (1-\mu^2)\cos\phi\sin\phi & \mu\sqrt{1-\mu^2}\cos\phi \\ (1-\mu^2)\cos\phi\sin\phi & (1-\mu^2)\sin^2\phi & \mu\sqrt{1-\mu^2}\sin\phi \\ \mu\sqrt{1-\mu^2}\cos\phi & \mu\sqrt{1-\mu^2}\sin\phi & \mu^2 \end{bmatrix}. \tag{22}$$

If we carefully choose the pole of $\mathbf{\Omega}$ to be the same direction as $\mathbf{b}$, the only dependence on ϕ in the integrand is contained in the tensor in Eq. 22, and all the off-diagonal terms integrate to zero. Eq. 21 becomes

$$\boldsymbol{\chi} = \frac{b}{4\pi \sinh b} \int_{-1}^{1} e^{b\mu} \begin{bmatrix} \pi\left(1-\mu^2\right) & 0 & 0 \\ 0 & \pi\left(1-\mu^2\right) & 0 \\ 0 & 0 & 2\pi\mu^2 \end{bmatrix} d\mu \,. \tag{23}$$

We really only have one more integral to do. Integrating by parts gives

$$\frac{b}{2\sinh b} \int_{-1}^{1} \mu^2 e^{b\mu} d\mu = \frac{b}{2\sinh b} \left[\left. \frac{\mu^2 e^{b\mu}}{b} \right|_{-1}^{1} - \frac{2}{b} \int_{-1}^{1} \mu e^{b\mu} d\mu \right] \tag{24}$$

$$= \left(1 - \frac{2}{b}\eta\right). \tag{25}$$

Using Eq. 25 in Eq. 23 gives

$$\boldsymbol{\chi} = \begin{bmatrix} \eta/b & 0 & 0 \\ 0 & \eta/b & 0 \\ 0 & 0 & 1-2\eta/b \end{bmatrix}. \tag{26}$$

This can be separated into an isotropic part and a beam part.

$$\boldsymbol{\chi} = \frac{\eta}{b} \begin{bmatrix} 1 & 0 & 0 \\ 0 & 1 & 0 \\ 0 & 0 & 1 \end{bmatrix} + \left(1 - 3\frac{\eta}{b}\right) \begin{bmatrix} 0 & 0 & 0 \\ 0 & 0 & 0 \\ 0 & 0 & 1 \end{bmatrix}. \tag{27}$$

But these tensors are in the coordinate system where the pole of $\mathbf{\Omega}$ is in the direction of $\mathbf{b}$, so we need to generalize them to

$$\boldsymbol{\chi} = \frac{\eta}{b}\mathbf{I} + \left(1 - 3\frac{\eta}{b}\right) \frac{\mathbf{b} \otimes \mathbf{b}}{b^2} \,. \tag{28}$$

In the one-dimensional case that we consider here, $\boldsymbol{\chi}$ degenerates to

$$\chi = 1 - 2\frac{\eta}{b} \,. \tag{29}$$

1.2 A APPROXIMATE ROE-TYPE RIEMANN SOLVER

Casting Eq. 1 into more a compact form, we write it as

$$\frac{\partial \mathbf{u}}{\partial t} + \frac{\partial \mathbf{F}\left(\mathbf{u}\right)}{\partial x} = \mathbf{S} \,, \tag{30}$$

where $\mathbf{u}(x,t) = \left[\phi(x,t), J(x,t)\right]^T$ is the state of the system at x and t, $\mathbf{F} = \left[J, \chi\phi\right]^T$ is the numerical flux, and $\mathbf{S} = \left[S_0 - \Sigma_a\phi, S_1 - \Sigma_t J\right]^T$ contains the source and collision terms. If we

integrate $\mathbf{u}(x,t)$ over a spatial cell and divide by Δx_i, we get space-averaged data in cell i at time t_n,

$$\mathbf{u}_i^n = \mathbf{u}_i(t_n) = \frac{1}{\Delta x_i}\int_{x_{i-1/2}}^{x_{i+1/2}} \mathbf{u}(x,t_n)\,dx\,. \tag{31}$$

Integrating Eq. 30 over space cell i and a time interval $\Delta t_n = t_{n+1} - t_n$ yields

$$\mathbf{u}_i^{n+1} - \mathbf{u}_i^n + \int_{t^n}^{t^{n+1}} \frac{\mathbf{F}\left(\mathbf{u}_{i+1/2}\right) - \mathbf{F}\left(\mathbf{u}_{i-1/2}\right)}{\Delta x_n} dt = \mathbf{S}_i^n\,, \tag{32}$$

where $\mathbf{u}_{i\pm1/2} = \mathbf{u}(x_{i\pm1/2},t)$. To proceed, we need some way to determine the numerical fluxes $\mathbf{F}\left(\mathbf{u}_{i\pm1/2}\right)$ for both the interior cells and at the system boundaries.

1.2.1 A Simplified Problem to Find the Numerical Fluxes

Upon integrating the system in Eq. 32, our approximation to $\mathbf{u}(x,t)$ is now piecewise continuous. It is possible to solve the problem locally at cell interfaces for short time intervals in order to determine the numerical flux $\mathbf{F}$. Consider the following source-free local problem for $\mathbf{u}(x,t)$,

$$\frac{\partial \mathbf{u}}{\partial t} + \frac{\partial \mathbf{F}\left(\mathbf{u}\right)}{\partial x} = 0 \tag{33}$$

with the initial condition

$$\mathbf{u}(x,0) = \begin{cases} \mathbf{u}_\ell & \text{if } x < 0 \\ \mathbf{u}_r & \text{if } x > 0\ . \end{cases} \tag{34}$$

In order to approximately solve the system (Eq. 33) of equations, we transform it into locally linearized characteristic variables. First, we introduce a Roe matrix, $\mathbf{A}(\mathbf{u}_\ell,\mathbf{u}_r)$, having the following properties:

- $\mathbf{A}(\mathbf{u}_\ell,\mathbf{u}_r)(\mathbf{u}_r - \mathbf{u}_\ell) = \mathbf{F}(\mathbf{u}_r) - \mathbf{F}(\mathbf{u}_\ell)$,
- As $\mathbf{u}_r, \mathbf{u}_\ell \to \mathbf{u}$, $\mathbf{A}(\mathbf{u}_\ell,\mathbf{u}_r)$ becomes the Jacobian of $\mathbf{F}(\mathbf{u})$, and
- $\mathbf{A}(\mathbf{u}_\ell,\mathbf{u}_r)$ is diagonalizable with real, distinct eigenvalues λ_k.

The first and second properties are necessary to obtain the correct net change of particles and momentum in each cell from one time step to the next. The third property is used in the transformation to characteristic variables.

We will then approximate Eq. 33 locally by replacing $\partial\mathbf{F}/\partial x$ with $\mathbf{A}(\mathbf{u}_\ell,\mathbf{u}_r)\partial\mathbf{u}/\partial x$ to yield

$$\frac{\partial \mathbf{u}}{\partial t} + \mathbf{A}(\mathbf{u}_\ell,\mathbf{u}_r)\frac{\partial \mathbf{u}}{\partial x} = 0\,. \tag{35}$$

The right and left eigenvectors of $\mathbf{A}$ are defined by

$$\mathbf{A}\mathbf{r}_k = \lambda_k \mathbf{r}_k \tag{36}$$

$$\mathbf{l}_k \cdot \mathbf{A} = \lambda_k \mathbf{l}_k \tag{37}$$

where k is the index of the eigenvalues; in a two moment closure like ours, there are only two eigenvalues.

To begin the transformation, we multiply Eq. 35 by $\mathbf{l}_k$

$$\mathbf{l}_k \cdot \frac{\partial \mathbf{u}}{\partial t} + \mathbf{l}_k \cdot \mathbf{A} \frac{\partial \mathbf{u}}{\partial x} = 0 \tag{38}$$

$$\frac{\partial a_k}{\partial t} + \lambda_k \mathbf{l}_k \cdot \frac{\partial \mathbf{u}}{\partial x} = 0 \tag{39}$$

$$\frac{\partial a_k}{\partial t} + \lambda_i \frac{\partial a_k}{\partial x} = 0 \tag{40}$$

where the characteristic variables $a_k = \mathbf{l}_k \cdot \mathbf{u}$. Decomposing the initial condition, Eq. 34, in the same way

$$a_k(x,0) = \begin{cases} a_k^\ell & \text{if } x < 0 \\ a_k^r & \text{if } x > 0 \end{cases} \tag{41}$$

allows us to write the solution of Eq. 40 as

$$a_k(x,t) = \begin{cases} a_k^\ell & \text{if } x - \lambda_k t < 0 \\ a_k^r & \text{if } x - \lambda_k t > 0 \,. \end{cases} \tag{42}$$

We can now reconstruct the solution, $\mathbf{u}(x,t)$, as

$$\mathbf{u}(x,t) = \sum_k a_k(x,t)\mathbf{r}_k \tag{43}$$

$$= \sum_{x-\lambda_k t<0} a_k^\ell \mathbf{r}_k + \sum_{x-\lambda_k t>0} a_k^r \mathbf{r}_k \,. \tag{44}$$

At $x = 0$ we have

$$\mathbf{u}(0,t) = \sum_{\lambda_k>0} a_k^\ell \mathbf{r}_k + \sum_{\lambda_k<0} a_k^r \mathbf{r}_k \,, \tag{45}$$

so finally we get $\mathbf{F}(\mathbf{u}(0,t))$

$$\mathbf{F}(\mathbf{u}(0,t)) = \mathbf{A}(\mathbf{u}_\ell, \mathbf{u}_r)\mathbf{u}(0,t) = \sum_{\lambda_k>0} \lambda_k a_k^\ell \mathbf{r}_k + \sum_{\lambda_k<0} \lambda_k a_k^r \mathbf{r}_k \,. \tag{46}$$

An important thing to notice is that the numerical flux at the interface $x = 0$ is independent of time. This enables us to complete the time integration in Eq. 32. If we view our initial data at each time step as a piecewise constant solution, we can apply the flux estimate from Eq. 46 to each of the cell interfaces, and thus advance to the next time level.

While the scheme presented here is only first order is space and time, it is easy to modify Roe-type Riemann solvers to be higher order in both space an time.[6,7]

1.2.2 Eigenstructure for Two Closures

A Roe matrix for P_1 theory is just

$$\mathbf{A} = \begin{bmatrix} 0 & 1 \\ 1/3 & 0 \end{bmatrix}, \tag{47}$$

with eigenvalues $\lambda_\pm = \pm 1/\sqrt{3}$. A Roe matrix for the maximum entropy approximation is harder to find, but we have found one, namely

$$\mathbf{A}(\mathbf{u}_\ell, \mathbf{u}_r) = \mathbf{A}(\eta_\ell, \eta_r) = \begin{bmatrix} 0 & 1 \\ \frac{\chi_\ell \eta_r - \chi_r \eta_\ell}{\eta_r - \eta_\ell} & \frac{\chi_r - \chi_\ell}{\eta_r - \eta_\ell} \end{bmatrix} \tag{48}$$

where $\chi_\ell = \chi(\eta_\ell)$, $\chi_r = \chi(\eta_r)$, $\eta_\ell = \eta(\mathbf{u}_\ell)$, and $\eta_r = \eta(\mathbf{u}_r)$. The eigenvalues are

$$\lambda_\pm = \frac{C}{2} \pm \sqrt{\frac{C^2}{4} + D} \tag{49}$$

where $C = (\chi_r - \chi_\ell)/(\eta_r - \eta_\ell)$ and $D = (\chi_\ell \eta_r - \chi_r \eta_\ell)(\eta_r - \eta_\ell)$. If we let $\eta_\ell, \eta_r \to \eta$ in Eq. 48, we get

$$\lim_{\eta_\ell, \eta_r \to \eta} \mathbf{A}(\eta_\ell, \eta_r) = \lim_{\eta_{\ell,r} \to \eta} \begin{bmatrix} 0 & 1 \\ \frac{\chi_\ell \eta_r - \chi_r \eta_\ell}{\eta_r - \eta_\ell} & \frac{\chi_r - \chi_\ell}{\eta_r - \eta_\ell} \end{bmatrix} \tag{50}$$

$$= \begin{bmatrix} 0 & 1 \\ \chi - \eta \frac{\partial \chi}{\partial \eta} & \frac{\partial \chi}{\partial \eta} \end{bmatrix}, \tag{51}$$

which is the Jacobian of $\mathbf{F}$. Proving that this matrix $\mathbf{A}$ also satisfies the first property of a Roe matrix, $\mathbf{A} \cdot (\mathbf{u}_\ell - \mathbf{u}_r) = \mathbf{F}_\ell - \mathbf{F}_r$, is straightforward algebra.

2 THE BOUNDARY CONDITIONS

In the Riemann solver, the numerical flux $\mathbf{F}$ is calculated at the cell interfaces, and we still need some way to specify $\mathbf{F}$ at the system boundaries. The first boundary condition described below is an implementation of the Mark[8,9] boundary condition, which specifies information coming into the system along specific directions. The second effectively implements the Marshak boundary condition, which specifies the incoming partial first moment. The third is an extension of the Marshak boundary condition which allows for the specification of extra information about the angular dependence of the incoming particles.

2.1 GHOST CELLS

The Riemann solver gives us a way to calculate the numerical flux, $\mathbf{F}$, across each of the cell interfaces. By placing ghost cells just outside the physical system, we transform the system boundaries into cell interfaces. In this cell we place a flux ϕ and current J which give the proper first and

second incoming partial moments for the closure we are using. The numerical flux across the system boundary is then calculated exactly like the numerical flux across the interior cell interfaces. In doing so, we specify the data to use for the incoming characteristic variables, a_k^ℓ (on the left boundary, or a_k^r on the right) for Eq. 46.

The Mark boundary conditions specify the value of the angular flux, $\psi(x, \mu, t)$ along particular directions. In P_1 theory these directions are $\mu = \pm 1/\sqrt{3}$ for the left and right boundaries, respectively. If we decompose $\mathbf{u}$ into the characteristic variables, we get

$$a_\pm = \mathbf{r}_\pm \cdot \mathbf{u} = \frac{1}{\lambda_\mp - \lambda_\pm} \begin{bmatrix} \lambda_\mp \\ -1 \end{bmatrix} \cdot \begin{bmatrix} \phi \\ J \end{bmatrix} = \frac{1}{2}\phi \pm \frac{\sqrt{3}}{2} J = \psi(\mu_\pm), \tag{52}$$

which are the angular fluxes in S_2. P_1 theory is equivalent to S_2 theory where all the neutrons travel along the two directions $\mu = \pm 1/\sqrt{3}$. The maximum entropy closure is similar, except the two characteristic directions depend on the state in the cells. The ghost cell method is thus essentially the Mark boundary condition for the maximum entropy closure and limits to the Mark boundary condition as the distribution becomes isotropic.

2.2 BOUNDARY EDDINGTON FACTOR

The boundary Eddington factor method,[10–12] simply called the boundary factor method here, is an implementation of the Marshak boundary condition, which specifies the partial incoming current. The boundary factor B is defined as

$$B = \frac{1}{\phi} \int_{-1}^{1} |\mu| \psi(\mu) d\mu \,, \tag{53}$$

which can be rewritten as

$$B\phi = \int_{-1}^{0} (-\mu)\psi(\mu) d\mu + \int_{0}^{1} \mu\psi(\mu) d\mu = -J^- + J^+. \tag{54}$$

For P_1 theory, $B = 1/2$. For the maximum entropy approximation, B is a function of η indirectly through b (see Eq. 4),

$$B = \frac{1 - \cosh b}{b \sinh b} + 1 \,. \tag{55}$$

Figure 2 plots B as a function of η for both P_1 and the maximum entropy approximation.

We need another equation to determine the two unknowns at the boundary, ϕ and J; another equation involving the partial first moments is

$$J = J^- + J^+. \tag{56}$$

To implement the boundary condition we first calculate the partial currents using the specified incoming partial current for the incoming data and the boundary cell data for the outgoing data.

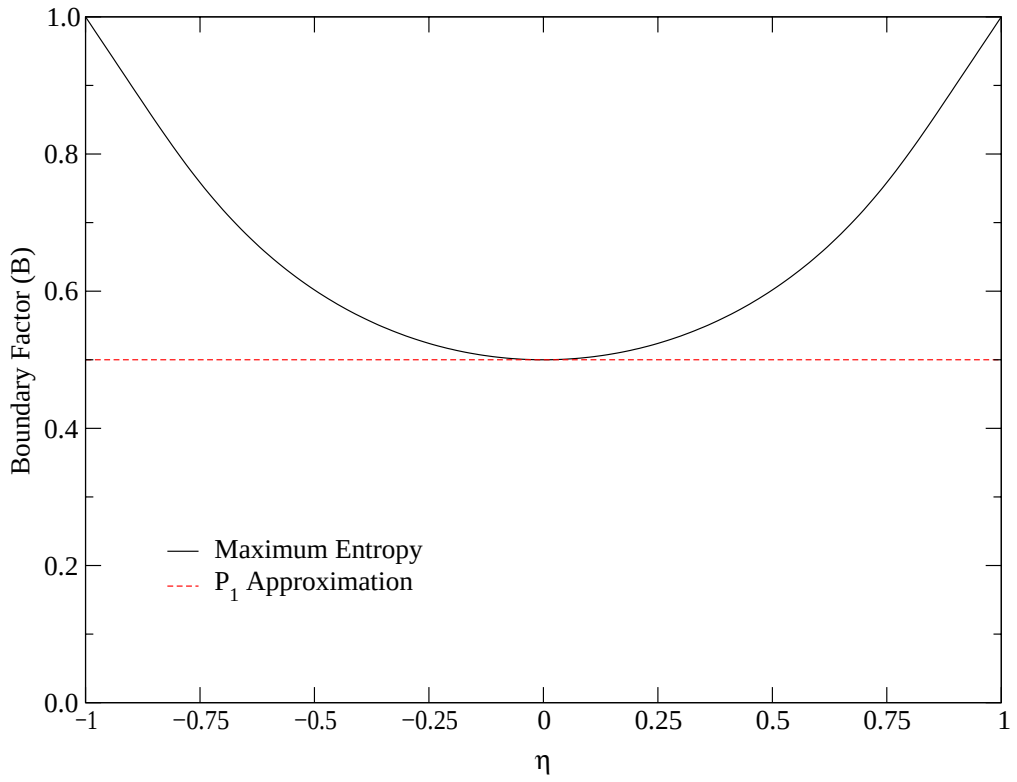

Figure 2: Boundary Factor as a function of $\eta = J/\phi$

The current, J, is then calculated from Eq. 56. In order to solve Eq. 54 efficiently, it is first normalized by J,

$$B(\eta)\frac{\phi}{J} = \frac{B(\eta)}{\eta} = \frac{-J^- + J^+}{J}\,. \tag{57}$$

We then have a function of η equal to a known value. We solve this for η, and then calculate $\phi = J/\eta$. This flux and current are then used to calculate a numerical flux $\mathbf{F}$ as $[J, \chi\phi]^T$ at the boundary. The only boundary data we need in this procedure is the incoming partial current.

As the cell size goes to zero and the cell values for ϕ and J approach the values at the boundary, this boundary condition becomes the standard Marshak boundary condition. At the left boundary, the positive partial current J^+ in the first cell becomes the specified positive current.

2.3 PARTIAL NUMERICAL FLUX

Explicitly writing the numerical flux $\mathbf{F}$ hints at another boundary condition.

$$\mathbf{F} = \int_{-1}^{1} \begin{bmatrix} \mu\psi \\ \mu^2\psi \end{bmatrix} d\mu = \int_{-1}^{0} d\mu \begin{bmatrix} \mu\psi \\ \mu^2\psi \end{bmatrix} d\mu + \int_{0}^{1} d\mu \begin{bmatrix} \mu\psi \\ \mu^2\psi \end{bmatrix} d\mu\,, \tag{58}$$

which can be rewritten as

$$\mathbf{F} = \begin{bmatrix} J^- \\ (\chi\phi)^- \end{bmatrix} + \begin{bmatrix} J^+ \\ (\chi\phi)^+ \end{bmatrix} = \mathbf{F}^- + \mathbf{F}^+ \tag{59}$$

where the $+$ indicates $\int_0^1 d\mu$ and the $-$ indicates $\int_{-1}^0 d\mu$. At the left boundary the incoming partial numerical flux, $\mathbf{F}^+$, is determined from a specified incoming angular flux, while the outgoing partial numerical flux, $\mathbf{F}^-$, is computed using the distribution found in the cell just inside the system. We then use the sum $\mathbf{F} = \mathbf{F}^- + \mathbf{F}^+$ to determine the net flow of stuff into the system at each boundary.

Inside the cell, we need to calculate the partial numerical flux for our distribution. The partial currents $J^\pm$ for P_1 theory are

$$J^\pm = \pm\frac{1}{4}\phi + \frac{1}{2}J\,, \tag{60}$$

while partial second moments $(\chi\phi)^\pm$ for P_1 theory are

$$(\chi\phi)^\pm = \frac{1}{6}\phi \pm \frac{3}{8}J\,. \tag{61}$$

For the maximum entropy approximation they are

$$J^\pm = \phi\frac{(b \mp 1)\, e^{\pm b} \pm 1}{2b\sinh b} \tag{62}$$

and

$$(\chi\phi)^\pm = \phi\frac{\pm e^{\pm b}\left(1 \mp b + \frac{b^2}{2}\right) + 1}{b^2\sinh b}\,, \tag{63}$$

respectively. With this boundary condition we can specify both the particle and momentum flow into the system (first and second moments).

3 RESULTS

These boundary conditions were used to solve for the scalar flux ϕ and the current J in a semi-infinite slab. The slab is five mean free paths thick, the scattering ratio is $c = 0.3$ in all but the last problem. The cell size was fixed at $\Delta x = 0.01$ mean free paths for all problems. Thick slabs have also been treated, but behave the same as in the results reported here and provide no new insight. Except where otherwise noted, the left side has an incident isotropic flux while the right side is a vacuum boundary.

Figure 3 shows the of the S_2 discrete ordinates method and the approximate Riemann solver applied to the P_1 equations. Using ghost cells, which provide the Mark boundary conditions, the scalar flux have the exact same shape as the S_2 calculation, The ghost cell calculated flux is about 0.61%

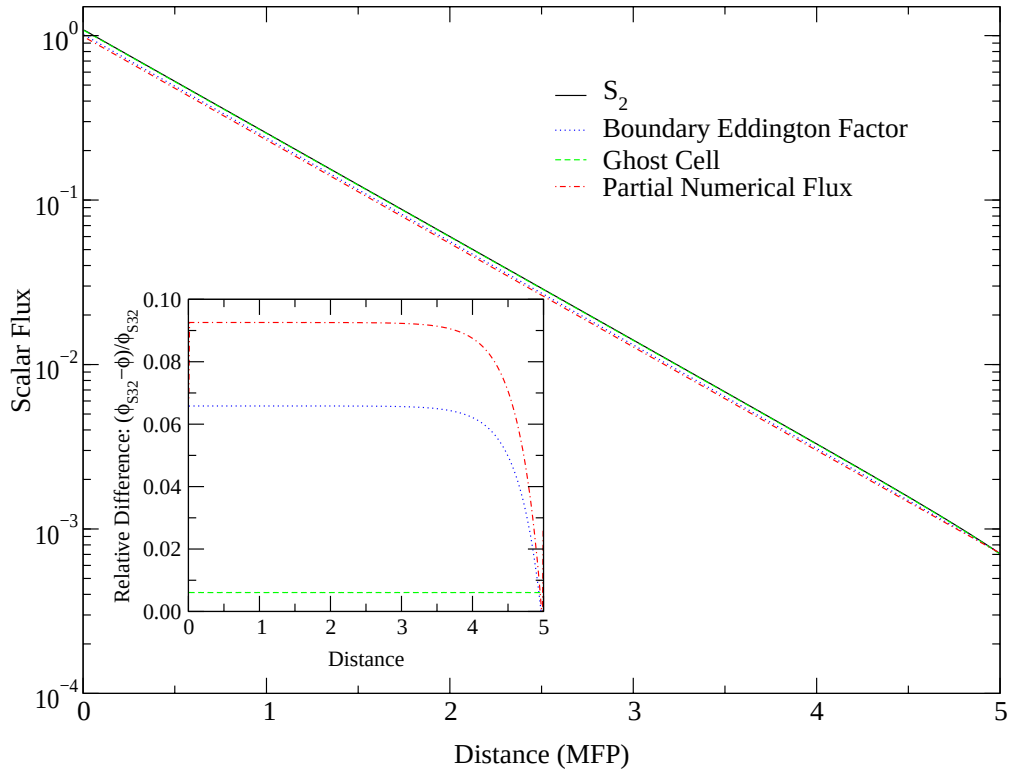

Figure 3: For P_1 theory and isotropic boundary conditions, the ghost cell method has the same shape as an S_2 calculation where the other two boundary conditions do not. The scattering ratio is $c = 0.3$.

too low, where the flux calculated with the boundary factor is about 6.6% too low and the partial numerical flux 9.2% low. A calculation with an incident incoming beam shows similar results.

The scalar flux calculated using the maximum entropy closure with the three different boundary conditions is compared to a S_{32} discrete ordinates method in Figure 4. Note here that the partial numerical flux boundary conditions yield a better solution, compared to transport, everywhere except the first half mean free path into the system.

There is a sharp jump in the boundary factor solution just inside the right boundary. In other studies we have discovered that the maximum entropy approximation changes character extremely rapidly in space as the material properties change. Here is it trying to be more isotropic near the edge due to the particle source, but changes rapidly to the infinite medium solution away from the boundary. At the vacuum boundary, the flux calculated using the boundary factor is too high and too isotropic.

Figure 5 shows that extra angular information about the incoming particles can be successfully introduced with the ghost cells and the partial numerical flux. A calculation similar to the ones above is made, but the scattering ratio is $c = 0.1$, and the boundary flux is either isotropic or a beam as indicated. The ghost cell method and the partial numerical flux produce almost identical results for the incident beam case.

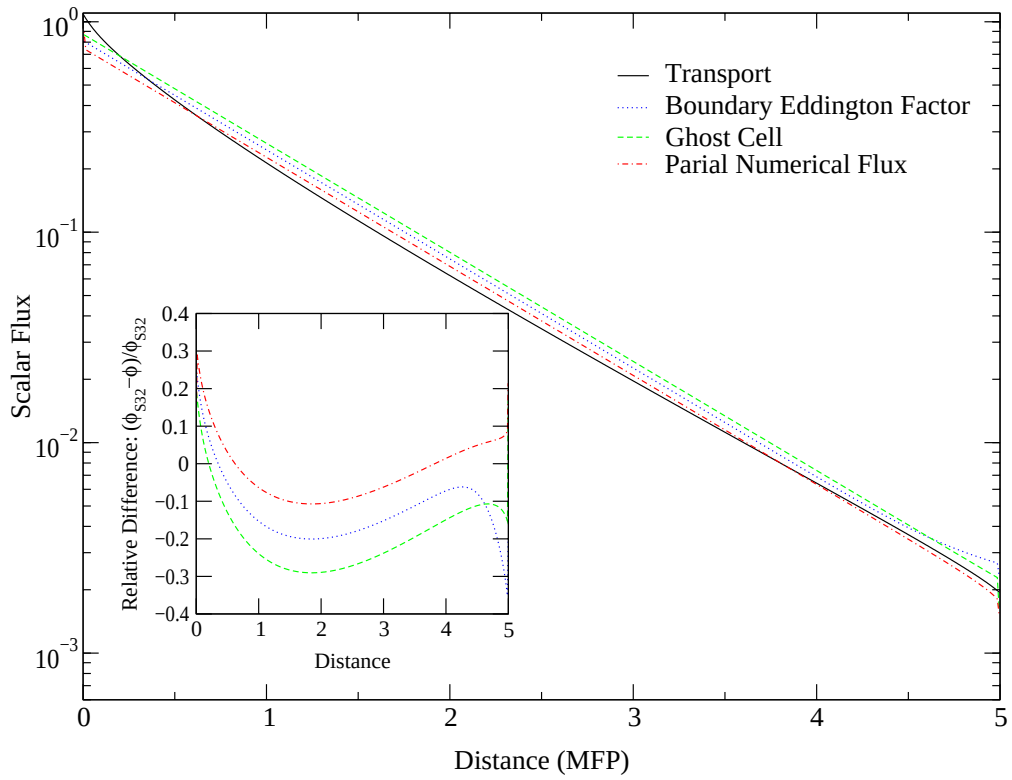

Figure 4: The various boundary conditions applied to a finite slab. The maximum entropy closure is compared to a S_{32} transport calculation. The inset shows the relative error produced by each of the boundary conditions compared to the transport calculated flux ϕ. The scattering ratio is $c = 0.3$.

4 CONCLUSIONS

The maximum entropy approximation is superior to the P_1 approximation (Figure 1); this was also seen in our previous results.[1,2] Overall, the maximum entropy solution using the partial numerical flux boundary condition yields better solutions than either the boundary factor or ghost cell boundary conditions. The ghost cell method, however, is extremely easy to implement and gives reasonable results. The boundary factor is especially bad at the vacuum boundary, where the solution is too isotropic. Only at boundaries where particles enter the system is the partial numerical flux inferior to the other methods, but within half a mean free path of the boundary the partial numerical flux solution is the best.

REFERENCES

1. T. A. Brunner, J. P. Holloway, and E. W. Larson, "On the use of maximum entropy eddington factors in shielding calculations," *Transactions of the American Nuclear Society*, vol. 77, pp. 195–196, Nov. 1997.

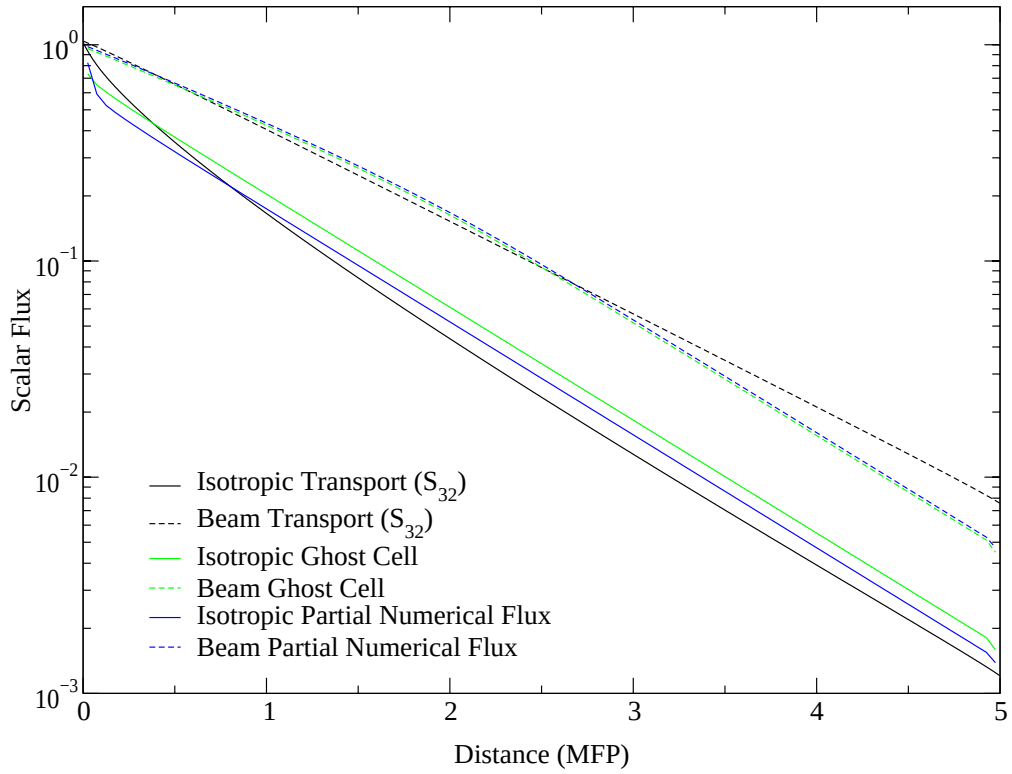

Figure 5: Scalar flux in a finite slab. The maximum entropy closure with ghost cells and partial numerical flux boundary conditions is compared to transport theory for an isotropic and beam incoming flux. The scattering ratio is $c = 0.1$.

2. T. A. Brunner, J. P. Holloway, and K. G. Powell, "Using an approximate riemann solver with the maximum entropy closure," *Transactions of the American Nuclear Society*, vol. 79, pp. 128–129, Nov. 1998.

3. G. N. Minerbo, "Maximum entropy eddington factors," *Journal of Quantitative Spectroscopy and Radiative Transfer*, vol. 20, p. 541, 1978.

4. R. J. LeVeque, *Numerical Methods for Conservation Laws*. Birkhäuser Verlag, 1992.

5. R. J. LeVeque, D. Mihala, E. A. Dorfi, and E. Müller, *Computational Methods for Astrophysical Fluid Flow*. Springer, 1998.

6. B. van Leer, W.-T. Lee, and K. G. Powell, "Sonic-point capturing," in *AIAA 9th Computational Fluid Dynamics Conference*, 1989.

7. P. Roe, "A brief introduction to high-resolution schemes," in *Upwind and High-Resolution Schemes* (M. Y. Hussaini, B. van Leer, and J. Van Rosendale, eds.), Springer, 1997.

8. G. I. Bell and S. Glasstone, *Nuclear Reactor Theory*. Krieger, 1970.

9. J. J. Duderstadt and L. J. Hamilton, *Nuclear Reactor Analysis*. John Wiley & Sons, Inc., 1976.

10. M. A. Cooper, *An Automated Variance Reducion Method for Global Monte Carlo Neutral Particle Transport Problems*. PhD thesis, University of Michigan, 1999.

11. M. M. Miften and E. W. Larson, "The quasi-diffusion method for solving transport problems in planar and spherical geometries," *Transport Theory and Statistical Physics*, vol. 22, pp. 165–186, June 1993.

12. M. M. Miften, *The Quasi-Diffusion Method for Transport Problems in Multidimensional Geometries*. PhD thesis, University of Michigan, 1994.